High-Speed Seismic Data Acquisition over mm-Wave Channels

Varun Amar Reddy*, Gordon L. Stüber†
Center for Energy and Geo Processing
School of Electrical & Computer Engineering
Georgia Institute of Technology
Atlanta, GA 30332, USA
*varun.reddy@gatech.edu, †stuber@ece.gatech.edu

Suhail I. Al-Dharrab
Center for Energy and Geo Processing
Electrical Engineering Department
King Fahd University of Petroleum & Minerals
Dhahran 31261, Saudi Arabia
suhaild@kfupm.edu.sa

***Abstract*—Wireless systems for seismic data acquisition offer several advantages over cable-based systems by reducing human impact on the environment and the costs associated with deployment, maintenance, and logistics. Millimeter-wave communication offers the requisite data rates to rapidly transfer large amounts of seismic data. A novel wireless geophone network architecture is described, based on the IEEE 802.11ad standard. A data collection scheme is also presented, resulting in a reduction of the total number of wireless gateways required in large-scale seismic surveys. Beamforming techniques are used to reduce co-channel interference, as per the geophone topology. Techniques for power conservation and propagation modelling are investigated. A performance evaluation in terms of the channel access scheme, throughput, and power consumption, is conducted on ns-3. The proposed wireless acquisition system provides a feasible and standards-compliant approach for deploying large-scale wireless geophone networks.**

***Index Terms*—wireless geophone networks, chain-type sensor networks, IEEE 802.11ad, millimeter wave, power saving.**

I. Introduction

Seismic surveys are conducted over large areas to keep up with the global demand for oil and gas. A seismic source generates waves that penetrate the ground and get reflected by subsurface layers. The reflected waves are recorded by geophones to obtain a graphic of the Earth's subsurface.

Seismic surveys typically deploy 10,000 to 30,000 geophones, covering an area of up to 100 km^2 [1]. A *sweep* is conducted by vibroseis trucks wherein large baseplates are used to generate seismic waves. The *sweep length* determines the duration of a sweep, ranging between 4 and 12 s. Geophones in the vicinity record data for a duration known as the *listen interval*. Typical geophones may generate data at a rate of 48 kbps, while three-component (3-C) geophones generate thrice the amount of data at a rate of 144 kbps. A network of 10,000 geophones can generate data at an aggregate rate as high as 1.4 Gbps.

Although cabled systems are reliable and effective, a significant amount of testing and maintenance work is required. Conducting a survey over a large area implies the need for extremely long cables, which in turn increases the equipment weight and labour cost. This work proposes to replace cables with a network of wireless geophones, resulting in a more economical and environment-friendly solution.

In [2], Savazzi et al. proposed a hierarchical wireless geophone network architecture and discussed the viability of using ZigBee, Bluetooth, Ultra-Wideband (UWB), WiFi, and WiMAX. In [3], Savazzi et al. described a wireless geophone network based on UWB along with a beaconing scheme for energy conservation. However, this approach may require the use of a large number of gateway nodes. A wireless architecture is described in [4] where seismic data is relayed serially through geophones using multiplexing schemes. While this approach is simple to implement, acquisition time may be high and nonuniform power consumption among the geophones is a cause for concern. Moreover, the above studies do not provide quantitative results. The authors in [5] proposed an architecture for relaying data through a chain-type sensor network and evaluated its performance. The cluster heads, however, are required to send data over large hop lengths and are subject to higher power consumption. In [6], the authors assessed the performance of a wireless architecture based on the IEEE 802.11af standard for seismic data acquisition. Although a standards-compliant architecture is proposed, a large antenna height for the geophones is required which may not be feasible in seismic surveys.

This work proposes to exploit the advantages of high data rates that can be obtained over mm-wave links, in order to reduce total acquisition time. A primary contribution of this work is a wireless architecture that can operate with a reduced number of gateway nodes and low geophone antenna heights, allowing for scalable operation of geophone networks with uniform power consumption over extremely large areas. The proposed architecture and data collection scheme are compliant with the IEEE 802.11ad standard, thereby facilitating easier deployment and reduction of costs associated with the use of licensed hardware. To study propagation characteristics, the two-ray ground reflection model is revisited at 60 GHz.

II. Overview of IEEE 802.11ad

The IEEE 802.11ad amendment [7], [8] creates several opportunities for high-speed data transfer in the 60 GHz

This work is supported by the Center for Energy and Geo Processing at Georgia Institute of Technology and King Fahd University of Petroleum and Minerals, under grant number GTEC1601.

band. The notion of a personal basic service set (PBSS) is introduced. A PBSS Control Point (PCP) coordinates communication between the stations in the PBSS. To ensure uniform power consumption among the stations, PCP handover is performed either implicitly or explicitly [7].

With a channel bandwidth of 2.16 GHz, data rates as high as 6 Gbps can be obtained. The standard operates on the Directional Multi-Gigabit (DMG) PHY, which further supports three types of PHY - Control, Single-Carrier (SC), and Orthogonal Frequency Division Multiplexing (OFDM). The concept of a virtual antenna sector is introduced, wherein antenna gain is obtained in a particular direction [7]. An optimal pair of antenna sectors is selected to improve the link budget.

The beacon interval is divided into the beacon header interval (BHI) and the data transmission interval (DTI). The DTI consists of either Contention-Based Access Periods (CBAPs) or Service Periods (SPs). Different types of channel access can be employed.

1) Contention-Based Access (CBA): Stations obtain channel access through carrier-sense multiple access with collision avoidance (CSMA/CA) during a CBAP. Inaccurate carrier sensing may occur wherein a station cannot detect transmissions occurring outside the range of its directional antenna.

2) Service Period Access (SPA): The PCP creates a schedule of SPs, wherein a pair of stations can communicate with one another during an SP. Since the schedule is broadcasted by the PCP during the BHI, stations can enter deep-sleep mode during those SPs when they are not operating.

3) Dynamic Service Period Allocation (DSPA): Stations are polled by the PCP, which respond with resource requests. Based on the resource requests, a schedule is drawn up by the PCP/AP and channel access is granted in the form of SPs.

III. Proposed Network Topology and Architecture

A popular type of acquisition geometry is an orthogonal arrangement [1]. Geophones are placed along straight lines called *Receiver Lines (RLs)*. In this study, a topology with an inter-geophone distance of 25 m along the RL is considered. The RLs are aligned parallel to one another, with a separation of 200 m. A total of 30 RLs, each comprising 480 geophones, creates a network encompassing an area of 72 km^2.

Fig. 1a provides an illustration of the proposed architecture based on the IEEE 802.11ad standard. A set of geophones are assigned to act as PCPs, as described in Section IV, and data is relayed through the PBSSs that are formed. Wireless Gateway Nodes (WGNs) are positioned along the RL to collect the amalgamated data. The WGNs are provided with an ample amount of storage and power resources. Ideally, all data is obtained at the WGN within the length of the next sweep. In order for data to be exchanged between adjacent PBSSs, a rapid association and disassociation (RAD) scheme is defined.

IV. Proposed RAD Scheme

Certain aspects of the IEEE 802.11ad standard can be exploited to meet the requirements of a geophone network.

A. Key Features

1) Directional Communication: Employing directional antennas along the RL can help eliminate co-channel interference from other RLs. The performance of carrier sensing is also improved, as all geophones are positioned along the RL.

2) Channel Access: The SPA scheme is ideal for use, since the delays associated with contention and polling are reduced. Additionally, there is an opportunity for power conservation.

3) Open Standard: The proposed architecture is standards-compliant. Functionality is implemented at the application and transport layers, leaving the IEEE 802.11ad PHY/MAC intact.

4) Power Saving: The use of the SPA scheme provided by the DMG MAC enables a geophone to enter deep-sleep mode during those SPs when it is not required to operate. A geophone can further conserve energy by initiating deep-sleep mode after all subsequent data has been relayed. In both cases, the sleep duration can be predetermined.

B. Operation

The operation of the RAD scheme consists of the *initialization* phase, followed by the *data transfer* phase. The initialization phase begins with the transmission of a control message from the central WGN. The control message is propagated along the RL by the formation of dynamic PBSSs through explicit PCP handover and association/disassociation of geophones with the said PBSSs. Although such a PCP handover scheme is not optimally coordinated and can lead to a high probability of collisions, the initialization phase is implemented prior to the start of the seismic surveying process, and is not time-sensitive. When the control message is received at the endmost geophone on the RL, G_a, an acknowledgment message is transmitted in response towards the central WGN. Additionally, an identifier is embedded in the final data packet of G_a, indicating to subsequent geophones along the RL that there is no further data available that will have to be relayed. The reception of the acknowledgment message at the WGN marks the end of the initialization phase. PCP assignment is implemented statically during the data transfer phase, wherein the control message (propagated during the initialization phase) instructs every n^{th} geophone to act as a PCP, and the other geophones to associate with the respective PCPs. The PBSSs operate on channels that are adjacent in frequency to minimize co-channel interference, as seen in Fig. 1a. After a sweep is completed and seismic data is ready for transmission from the geophones, the following steps are implemented during the data transfer phase:

1) With the assigned PBSSs in place, data transfer begins through the SPA scheme. For instance, in Fig. 1a, data is relayed from G_a to G_b in PBSS P_a and from G_c to G_d in PBSS P_b[1]. Geophones enter deep-sleep mode during an SP when their operation is not required.
2) Upon reception of all data within the PBSS, G_b and G_d request to be disassociated from P_a and P_b respectively.

[1]Simultaneous operation occurs in the other PBSSs shown to the right of the WGN in Fig. 1; their notations are not specified to avoid overemphasis.

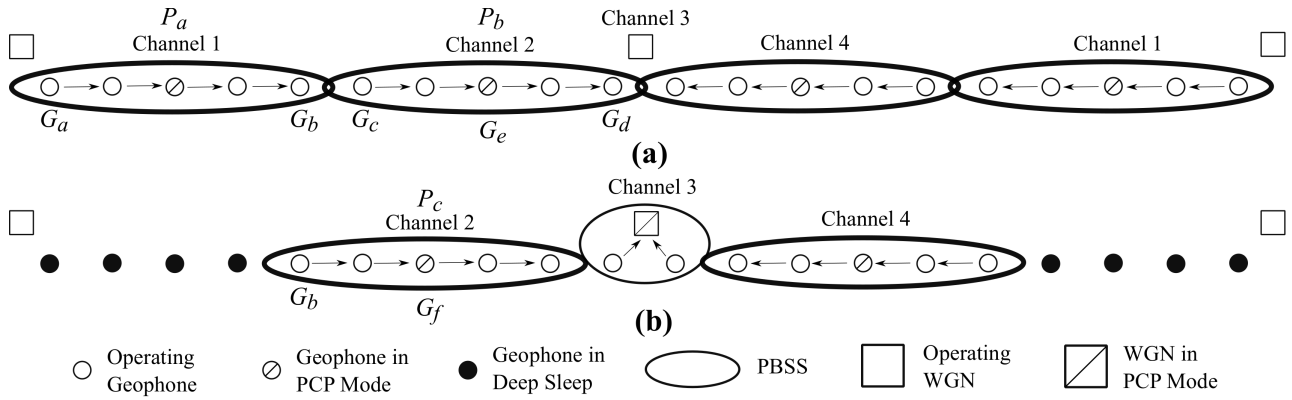

Fig. 1: Working of the RAD Scheme: (a) Geophones within P_a and P_b relay data towards the end of the PBSS. (b) G_b and G_d join newly formed PBSSs to relay the previously collected data towards the WGN.

3) The PCP G_e grants the disassociation request of G_d, and selects an adjacent geophone G_f to take on its role through explicit handover, resulting in the formation of a new PBSS P_c as seen in Fig. 1b.
4) After disassociation from P_a, G_b scans the adjacent channel for beacon frames and associates itself with P_c. The amalgamated data of P_a is then relayed from G_b through the geophones in P_c. A similar procedure is executed by G_d after disassociating from P_b.
5) If an identifier from G_a is detected and relayed, as in the case of P_a, the PCP instructs all currently associated geophones to enter deep-sleep mode, and are scheduled to wake up in time for the next sweep.
6) Steps (2) through (5) are repeated in additional PBSSs along the RL, until the data is delivered to the nearest WGN.
7) At the end of the next sweep, steps (1) through (6) are repeated with data being relayed in the opposite direction, in order to ensure uniform power consumption over several sweeps. In this case, data is relayed towards the WGNs positioned at the ends of the RL.

V. Propagation Modelling

Several studies have been conducted to characterize path loss in the mm-wave spectrum in outdoor and indoor environments [9], [10]. However, these models do not apply to the environments that typically occur in a seismic survey area. Moreover, the antennas are considered to be several meters above the ground in existing studies.

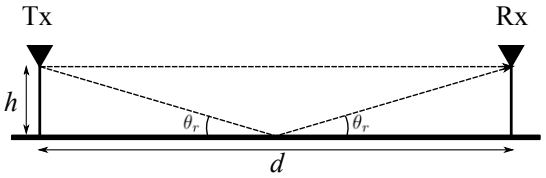

Fig. 2: The two-ray propagation model as applied to geophones with equal antenna heights [11].

The use of a near-ground propagation model is required for geophone networks, where the impact of ground reflection becomes significant, as shown in Fig. 2. The use of the two-ray propagation model [11] in mm-wave bands is validated in [12], [13]. The two-ray path loss L_{tr} can be expressed as -

$$L_{\text{tr}}[\text{dB}] = 20 \cdot \log_{10}\left[\left(\frac{4\pi d}{\lambda_c}\right)\left|1 + \Gamma_{\perp} e^{j\Delta\phi}\right|^{-1}\right] \quad (1)$$

where d is the distance between the transmitter and receiver in meters, λ_c is the wavelength in meters, $\Delta\phi$ is the phase difference in radians, and $\Gamma_{\perp}$ is the reflection coefficient corresponding to perpendicularly polarized signals. For a short geophone antenna height, $h \ll d$ and $\Delta\phi \approx (4\pi h^2)/(\lambda_c d)$. Furthermore, $\Gamma_{\perp}$ is related to the complex permittivity ϵ as -

$$\Gamma_{\perp} = \frac{\sin(\theta_r) - \sqrt{\epsilon - \cos^2(\theta_r)}}{\sin(\theta_r) + \sqrt{\epsilon - \cos^2(\theta_r)}} \quad (2)$$

The permittivity and conductivity of the ground depend on the frequency of the reflected wave [13]. Fig. 3a depicts the variation of $\Gamma_{\perp}$ with distance for reflection off dry ground (ϵ = $3 - 0.217j$) at 60 GHz and $h = 0.2$ m.

In the 60 GHz range, an additional path loss L_{ga} arises from gaseous absorption [14], and is expressed as -

$$L_{\text{ga}}[\text{dB}] = (\gamma_o + \gamma_w) \cdot d' \quad (3)$$

where γ_o and γ_w are the specific attenuation of oxygen and water vapour respectively, and d' is the path length in meters. For short antenna heights, $h \ll d$ and $d' \approx d$. Fig. 3b illustrates the variation of path loss at 60 GHz, $h = 0.2$ m in dry air (γ_o = 0.017 dB/m [14]) and reflection off dry ground. The impact of L_{ga} becomes significant only for distances greater than 100 m.

Fig. 3c depicts the variation of L_{tr} at 60 GHz as a function of the geophone antenna height, for distances that are multiples of 25 m. Successive fades are seen to occur over small intervals of antenna height, suggesting that the environmental height can have a significant impact.

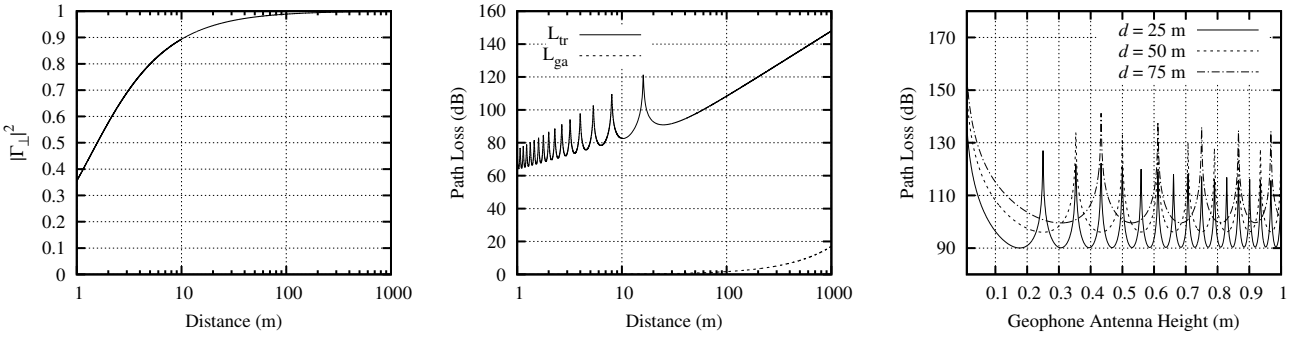

(a) Reflection Coefficient (b) Path Loss at 60 GHz (c) Two-Ray Path Loss vs. Antenna Height

Fig. 3: Propagation modelling for wireless geophone networks.

VI. Performance Evaluation

The performance of the proposed architecture is evaluated for a single sweep. The impact of co-channel interference up to the second tier is analyzed, given a 4-cell reuse pattern.

A. Simulation Setup

The ns-3 simulator is used for evaluation [15]. The simulation parameters are listed in Table I. An open-area flat-land environment is considered, and the path loss is modelled as per the discussion in Section V. The network is initialized as per the RAD scheme. Comparisons are drawn between the IEEE 802.11ad channel access schemes in order to demonstrate the superiority of the SPA scheme with respect to power conservation. All geophones are allocated SPs of equal duration. The DSPA scheme is not evaluated, as its performance is strongly dependent on the scheduling algorithm; the design of a scheduler is outside the scope of this work. Parameters pertaining to chipsets suitable for use in IEEE 802.11ad devices are described in [16]. The data collection performance from 240 geophones at a single WGN is analyzed.

B. Simulation Results

Fig. 4 describes the performance of the proposed architecture and the RAD scheme. Geophone antenna heights are selected in accordance with Fig. 3c and to counter co-channel interference. It is seen that a PBSS cannot contain more than 5 geophones, as an additional geophone would lie outside the maximum range of the PCP. The given system is noise-limited, as signal bandwidth is large at the receiver and co-channel interference is subdued by path loss and loss due to gaseous absorption at distances greater than 100 m.

In Fig. 4a, the total time required to relay all data to the WGN is plotted. For a PBSS size of two, a large number of handovers are required to reach the WGN, which introduces a significant delay. The total time taken drops to a much lower value for a PBSS size of three, owing to a reduction in the number of required handovers. From thereon, the impact of the time taken for data transfer within a PBSS becomes more prominent, as compared to the time taken for PCP handover. A larger PBSS implies more number of hops until the data is relayed to the endmost geophone. Consequently, there is an increase in the time taken with the number of geophones in a PBSS. Additionally, the SPA scheme is seen to execute better performance by reducing overhead due to collisions and contention. The variation of the throughput at the WGN in Fig. 4b can be explained on similar grounds.

In Fig. 4c, the advantage of the SPA scheme over the CBA scheme in terms of average power consumption per geophone is shown. Apart from the power that is conserved by mitigating the effects of contention, geophones enter deep-sleep mode as per the SP schedule that is broadcasted by the PCP. This helps to conserve up to 29.7% of power, as compared to the CBA scheme. Further power is conserved by the geophones by entering deep-sleep mode after all data has been relayed.

The use of a PBSS size of 5 is the most ideal scenario as power conservation is maximized while being able to collect all data within the sweep length. Thus, a total of 90 WGNs (3 WGNs per RL) would be sufficient for a seismic survey spanning an area of 72 km^2, as discussed in Section III.

TABLE I: Simulation Parameters

Parameter	Value	Parameter	Value
Operating Frequency	60.48 GHz	Noise Figure	7 dB
Bandwidth	2.16 GHz	Control PHY Data Rate (MCS0)	27.5 Mbps
Listen Interval	6 s	SC PHY Data Rate (MCS1)	385 Mbps
Sweep Length	8 s	Frame Aggregation	Enabled
Geophone Data Rate	144 kbps	Wifi Manager	Constant Rate
Geophone Antenna Height	0.17 - 0.31 m	Current (Idle Mode)	465 mA
Maximum Transmit Power	10 dBm	Current (Transmit Mode)	661 mA
Maximum Antenna Gain	24 dB	Current (Receive Mode)	533 mA
Receiver & CCA Sensitivity	-78 dBm	Current (Sleep Mode)	33 mA

C. Comparison with prior work

In Fig. 5, the performance of the architecture based on the IEEE 802.11af standard [6] is compared with the proposed architecture, given the same topology and a 4-cell reuse pattern. It is seen that the proposed architecture requires a far less number of WGNs to map the entire survey area, in

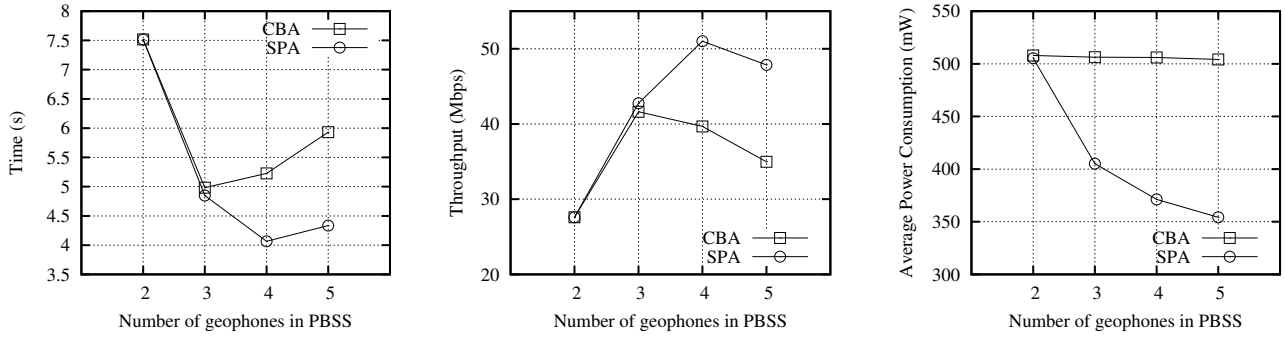

(a) Total Time Taken for Data Transfer (b) Throughput at WGN (c) Average Power Consumption

Fig. 4: Performance evaluation in terms of total time taken, throughput, and average power consumption.

addition to a significantly lower geophone antenna height. However, the average power consumption of the geophones is nearly 23% higher. A large bandwidth coupled with the need for directional communication leads to an increase in the power consumed. Moreover, the initialization phase of the RAD scheme is more complex than the set up required in [6].

VII. Conclusion

A wireless geophone network based on the IEEE 802.11ad standard is described and evaluated. The proposed RAD scheme greatly reduces the required number of gateway devices and geophone antenna height. The impact of co-channel interference is subdued with the help of directional communication. Despite the challenges presented by a dense network of geophones deployed over a large area, a scalable architecture with a low gateway density of 1.25 WGNs/km^2 has been shown to perform well. Power is conserved in the SPA scheme by placing geophones in deep-sleep mode when they are not operating. Uniform power consumption among geophones is ensured by alternating the direction of data transfer along the RL. Despite the use of power saving schemes, the geophones draw more power as compared to earlier studies. The findings presented in this work can also be applied to other categories of dense chain-type wireless sensor networks.

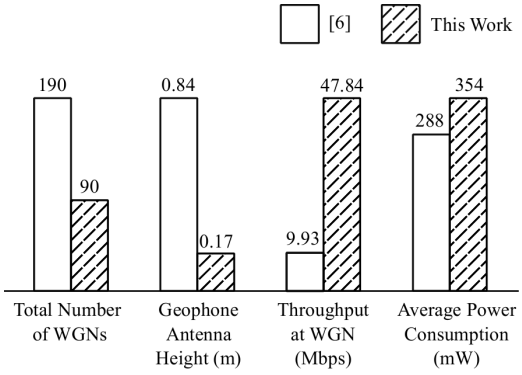

Fig. 5: Comparison between IEEE 802.11af-based and IEEE 802.11ad-based geophone network architectures.

References

[1] G. Vermeer, *3D Seismic Survey Design*, 2nd ed. Society of Exploration Geophysicists, 2012.

[2] S. Savazzi and U. Spagnolini, "Wireless geophone networks for high-density land acquisition: Technologies and future potential," *The Leading Edge*, vol. 27, no. 7, pp. 882–886, 2008.

[3] S. Savazzi, U. Spagnolini, L. Goratti, D. Molteni, M. Latva-aho, and M. Nicoli, "Ultra-wide band sensor networks in oil and gas explorations," *IEEE Communications Magazine*, vol. 51, no. 4, pp. 150–160, April 2013.

[4] Douglas B. Crice, "Systems and methods for seismic data acquisition," *U.S. Patent 9,291,732*, March 2016.

[5] C. W. Chen and Y. Wang, "Chain-Type Wireless Sensor Network for Monitoring Long Range Infrastructures: Architecture and Protocols," *Int. J. Distrib. Sen. Netw.*, pp. 287–314, Oct. 2008.

[6] V. A. Reddy, G. L. Stüber, and S. Al-Dharrab, "Energy Efficient Network Architecture for Seismic Data Acquisition via Wireless Geophones," in *IEEE International Conference on Communications (ICC)*, Kansas City, USA, May 2018.

[7] "IEEE 802.11ad, Amendment 3: Enhancements for Very High Throughput in the 60 GHz Band," pp. 1–628, Dec 2012.

[8] T. Nitsche, C. Cordeiro, A. B. Flores, E. W. Knightly, E. Perahia, and J. C. Widmer, "IEEE 802.11ad: Directional 60 GHz Communication for Multi-Gigabit-per-Second Wi-Fi," *IEEE Communications Magazine*, vol. 52, no. 12, pp. 132–141, December 2014.

[9] 3GPP TR 38.900 v14.3.1, "Study on channel model for frequency spectrum above 6 GHz," *Tech. Rep.*, 2017.

[10] T. S. Rappaport, Y. Xing, G. R. MacCartney, A. F. Molisch, E. Mellios, and J. Zhang, "Overview of Millimeter Wave Communications for Fifth-Generation (5G) Wireless Networks - with a Focus on Propagation Models," *IEEE Transactions on Antennas and Propagation*, vol. 65, no. 12, pp. 6213–6230, Dec 2017.

[11] G. L. Stüber, *Principles of Mobile Communication*, 4th ed. Springer International Publishing, 2017.

[12] E. Zöchmann, K. Guan, and M. Rupp, "Two-ray models in mmwave communications," in *2017 IEEE 18th International Workshop on Signal Processing Advances in Wireless Communications*, July 2017, pp. 1–5.

[13] S. Jaeckel, L. Raschkowski, S. Wu, L. Thiele, and W. Keusgen, "An explicit ground reflection model for mm-wave channels," in *2017 IEEE Wireless Communications and Networking Conference Workshops*, March 2017, pp. 1–5.

[14] ITU-R P.676-11, "Attenuation by atmospheric gases," *Tech. Rep.*, 2016.

[15] H. Assasa and J. Widmer, "Implementation and Evaluation of a WLAN IEEE 802.11ad Model in Ns-3," in *Proceedings of the Workshop on Ns-3*, ser. WNS3 '16. ACM, 2016, pp. 57–64.

[16] M. Boers, B. Afshar, I. Vassiliou, S. Sarkar, S. T. Nicolson, E. Adabi, B. G. Perumana, T. Chalvatzis, S. Kavvadias, P. Sen, W. L. Chan, A. H. T. Yu, A. Parsa, M. Nariman, S. Yoon, A. G. Besoli, C. A. Kyriazidou, G. Zochios, J. A. Castaneda, T. Sowlati, M. Rofougaran, and A. Rofougaran, "A 16TX/16RX 60 GHz 802.11ad Chipset With Single Coaxial Interface and Polarization Diversity," *IEEE Journal of Solid-State Circuits*, vol. 49, no. 12, pp. 3031–3045, Dec 2014.